metals

MDPI

Article

Effect of B and N Content and Austenitization Temperature on the Tensile and Impact Properties of Modified 9Cr-1Mo Steels

Ravindran Rejeesh [1,*], Rakesh Kumar Barik [1], Rahul Mitra [1], Andrii Kostryzhev [2], Chitta R. Das [3,4], Shaju K. Albert [3,4] and Debalay Chakrabarti [1]

[1] Indian Institute of Technology (IIT), Kharagpur 721302, India; barikrakesh4@iitkgp.ac.in (R.K.B.); rahul@metal.iitkgp.ac.in (R.M.); debalay@metal.iitkgp.ac.in (D.C.)
[2] The Center for Microscopy and Microanalysis, University of Queensland, Brisbane 4072, Australia; a.kostryzhev@uq.edu.au
[3] Indira Gandhi Center for Atomic Research (IGCAR), Kalpakkam 603102, India; chitta@igcar.gov.in (C.R.D.); shaju@igcar.gov.in (S.K.A.)
[4] Homi Bhabha National Institute, Kalpakkam 603102, India
* Correspondence: rejeeshsankaralil@iitkgp.ac.in; Tel.: +91-9447782729

Abstract: The present study investigates the relative effect of B and N concentrations and the austenitization temperature on the microstructure and mechanical properties (tensile and Charpy impact) of modified 9Cr-1Mo (P91) steels. Initially, a B-free P91 steel (with 500 ppm N) and four different B-containing steels (25–100 ppm) with varying N concentrations (20–108 ppm) were hot-rolled, normalized from different austenitization temperatures (1000–1100 °C/1 h) and finally tempered at 760 °C for 1 h. A Charpy impact test shows that the ductile–brittle transition temperature (*DBTT*) of all the B-added steels decreases with an increase in the austenitization temperature, where the 100 ppm B steel offers the lowest *DBTT* (−85 °C). Similarly, the strength increases with the increase in the austenitization temperature (1100 °C), with a slight drop in ductility. The influence of precipitates on the microstructure and mechanical properties is explained considering the B enrichment at the precipitates and the thermodynamic stability of the precipitates. The 100 ppm B steel (containing the maximum B and minimum N), normalized from 1100 °C austenitization, shows the best combination of tensile and Charpy impact properties, owing to the effective dissolution of coarse $M_{23}C_6$ and MX precipitates during the normalization treatment and the formation of fine B-rich $(Fe,Cr)_{23}(B,C)_6$ precipitates during the subsequent tempering.

Keywords: modified P91 steels; B and N contents; austenitization temperature; auger electron spectroscopy; precipitate stability; microalloyed MX precipitates; tensile testing; impact properties

check for updates

Citation: Rejeesh, R.; Barik, R.K.; Mitra, R.; Kostryzhev, A.; Das, C.R.; Albert, S.K.; Chakrabarti, D. Effect of B and N Content and Austenitization Temperature on the Tensile and Impact Properties of Modified 9Cr-1Mo Steels. *Metals* **2023**, *13*, 1124. https://doi.org/10.3390/met13061124

Academic Editor: Andrey Belyakov

Received: 28 May 2023
Revised: 8 June 2023
Accepted: 13 June 2023
Published: 15 June 2023

Copyright: © 2023 by the authors. Licensee MDPI, Basel, Switzerland. This article is an open access article distributed under the terms and conditions of the Creative Commons Attribution (CC BY) license (https://creativecommons.org/licenses/by/4.0/).

1. Introduction

Boron-added-modified 9Cr-1Mo (P91) steel is suitable for use as a structural component of steam generators and boilers considering its excellent oxidation resistance and superior creep rupture strength at elevated temperatures, along with its good tensile strength [1,2]. Although these steels are subjected to irradiation, impact toughness remains an important requirement for ensuring structural integrity. Particularly, it is necessary to understand whether the addition of B and N has any adverse effect on the impact toughness. Ensuring sufficient toughness and avoiding hydrogen-assisted cracking (HAC) are among the significant technological obstacles encountered during the welding process of 9Cr-1Mo steel [3,4].

Some recent studies on the effect of the composition have led to the development of the P92 grade steels, where some fraction of Mo in the P91 steel is replaced by tungsten (W) containing tungsten (W) with a lower fraction of Mo compared to P91 steel developed to achieve better mechanical properties and a higher creep rupture strength [5]. These benefits make the 9% Cr steel a dependable option for demanding applications in sectors with

high temperatures and high levels of stress. The higher chances of laves phase nucleation and rapid growth during long-term aging also play a key role in the variation in the static mechanical properties of P92 steels [6]. Apart from the steel grades containing 9 wt.% Cr, some research has also been devoted to studying the influence of zirconium (Zr) and hafnium (Hf) addition in refining the precipitates (mostly the oxide particles) in 14 wt.% Cr and 16 wt.% Cr steels, respectively, to improve both the strength and ductility [7,8]. The improved strength–toughness combination was mainly attributed to the stronger bonding force at the interface between the fine particles and matrix, as well as the increased hindrance provided by the smaller particles against dislocation movements.

Besides the steel composition, the heat treatment schedule, particularly the austenitization temperature, also plays an important role in regulating the impact toughness of high-Cr steels. Chatterjee et al. [9,10] studied the effect of the austenitization temperature (950–1100 °C) on the ductile-to-brittle transition behavior of B-free P91 steel by performing Charpy impact testing. It was found that the austenitization treatment at an intermediate temperature of 1025 °C improved the impact properties due to a smaller 'effective grain size', a higher fraction of high-angle boundaries, the presence of a beneficial γ-fiber texture and the dissolution of the pre-existing coarse precipitates. Pandey et al. [11] performed a similar study on B-free P91 grade steel and found that an increase in the normalizing temperature (from 950 °C to 1150 °C) resulted in a decrease in toughness (particularly above 1050 °C), primarily due to the coarsening of $M_{23}C_6$ precipitates, which promotes the cracking of secondary particles and de-cohesion at the precipitate/matrix interface. Such studies are rare in the same grade of steel with different B and N concentrations, which are expected to influence the precipitate coarsening and dissolution during the austenitization treatment.

In general, B is added in high-strength, low-C bainitic/martensitic steels for increasing the hardenability by segregating at the prior austenite grain (PAG) boundaries and thereby suppressing the nucleation of ferrite and pearlite at those sites [12,13]. Such a phenomenon is certainly beneficial in 9Cr-1Mo steel with a tempered martensitic microstructure, as B segregation can strengthen the PAG boundaries, preventing the local softening at those locations during high-temperature exposure. B significantly reduces the coarsening rate of $M_{23}C_6$ precipitates by forming fine and stable boro-carbides by partially replacing C with B, which provides a stronger pinning effect of grain boundaries and sub-grain boundaries [14–23]. In addition to $M_{23}C_6$-type precipitates, MX precipitates (M = V and/or Nb, X = C and/or N) also play a vital role in strengthening. Moreover, the presence of a high amount of N in P91 steel can easily form enough fine and stable MX nitrides which contribute to creep resistance [24–26]. However, excess N can also form brittle BN particles, which act as crack initiation sites [27,28]. Therefore, an optimum concentration of B and N is necessary for improving the creep strength of P91 steel. Our recent work [19] showed that, in base steels containing high B (70–100 ppm), a considerably higher N content (90–110 ppm) is beneficial for creep resistance (contributed by fine and stable MX nitrides) compared to a low N content (20 ppm).

Limited studies have been carried out on the impact toughness of B-containing high-Cr steels. Usually, B is found to be detrimental to the impact toughness of these steels by promoting a temper embrittlement phenomenon due to the stabilization and coagulation of $M_{23}(B,C)_6$ precipitates along the PAG boundaries or lath boundaries [29,30]. In addition, Mishnev et al. [30] observed a deterioration in the impact toughness of 10% Cr-containing steel with an increase in the B content (from 0 to 80 ppm) and a decrease in the N content (from 500 ppm to 30 ppm) due to the formation of chains of closely spaced $M_{23}C_6$ carbides along the lath boundaries. The nucleation of micro-voids from those closely spaced precipitates leads to early void coalescence and cracking. However, the exact effect of N on influencing the toughness is not deliberated in this study.

The present study aims to investigate the synergetic effect of B and N concentrations and the austenitization temperature on the microstructure and tensile and impact properties of modified 9Cr-1Mo steel.

2. Materials and Methods

2.1. Steel Composition

Five different steel grades of modified 9Cr-1Mo steel (B-free and B-added P91 steels) were prepared by an Indian manufacturer following identical vacuum induction melting and casting practices, each grade weighing between 10 and 15 kg (also detailed in our previous work [19]). The chemical compositions of all the prepared steels were determined using optical emission spectroscopy (OES), which are provided in Table 1. The B-free steel is a standard modified 9Cr-1Mo steel that contains a high amount of N (500 ppm), prepared according to the ASTM A213 (or ASME SA213) specifications [31]. On the other hand, in the remaining B-containing steels, different combinations of low-B medium-N (25 ppm B and 90 ppm N), medium-B high-N (70 ppm B and 108 ppm N), high-B medium-N (90 ppm B and 90 ppm N) and high-B low-N (100 ppm B and 20 ppm N) were used for a better understanding of the relative effect of both of the alloying elements. Steels are named after the amount of B addition, e.g., B-free, 25 ppm B, 70 ppm B, 90 ppm B and 100 ppm B (Table 1). The B and N concentrations are chosen in such a way that a controlled compositional variation can be achieved by avoiding the harmful BN formation, which is considered as a potential crack initiator that can deteriorate the steel toughness. To prevent the BN formation, we adhered to the BN solubility curve [19] derived from Equation (1), following [27]. Additionally, all of the other alloying elements in the steel are kept within the standard specification range.

$$\log[\text{wt.\%B}] = 2.45 \log[\text{wt.\%N}] - 6.81 \quad (1)$$

Table 1. Composition of investigated steels (wt.%).

Elements (wt.%)	C	Cr	Mo	Mn	Si	V	Nb	S	P	Ni	Al	Ti	N	B
B-free	0.10	8.93	0.86	0.41	0.21	0.20	0.08	0.005	0.020	0.20	0.010	-	0.050	-
25 ppm B	0.13	8.65	1.06	0.22	0.11	0.24	0.11	0.006	0.02	0.08	0.003	-	0.009	0.0026
70 ppm B	0.15	9.35	0.98	0.37	0.33	0.11	0.10	0.004	0.002	0.05	0.004	0.002	0.011	0.0070
90 ppm B	0.11	8.70	0.96	0.25	0.10	0.25	0.08	0.007	0.02	0.11	0.002	-	0.009	0.0090
100 ppm B	0.10	8.50	1.00	0.30	0.40	0.23	0.09	0.002	0.005	0.02	0.030	-	0.002	0.0100

2.2. Material Processing and Characterization

The as-cast ingots were homogenized at 1250 °C, hot-forged and hot-rolled (finish-rolled at ~1050 °C) to 10 mm thick plates. The normalization (N) treatment comprised austenitization at 1000/1050/1100 °C for 1 h and air-cooling followed by tempering (T) at 760 °C for 1 h. Details of the heat treatment schedule can be found in [19].

Detailed microstructural characterization was performed on the RD-ND plane of the heat-treated plates (shown in Figure 1 and also reported in our previous article [19]), which includes optical microscopy, scanning electron microscopy (SEM), transmission electron microscopy (TEM) and auger electron spectroscopy (AES) techniques. The details of all the characterization techniques employed are provided in our previous article [19].

2.3. Tensile and Charpy Impact Testing

Tensile specimens were fabricated from the heat-treated plates as per the ASTM E8 standard [32] and were tested at room temperature with a strain rate of 3.3×10^{-4} s^{-1} using an Instron servo hydraulic test system with a 100 kN load capacity. Standard Charpy V-notch specimens were fabricated and tested in a 400 J capacity pendulum-type machine following ASTM E23 [33] at different temperatures over the range of +100 °C to −196 °C. The dimensions and orientations of the tensile and Charpy impact specimens, extracted from the rolled and heat-treated plates, are shown in Figure 1. As a note, for both the tensile and Charpy tests, three specimens were evaluated under each testing

condition, and the reported properties represent the average results obtained for each heat-treatment condition.

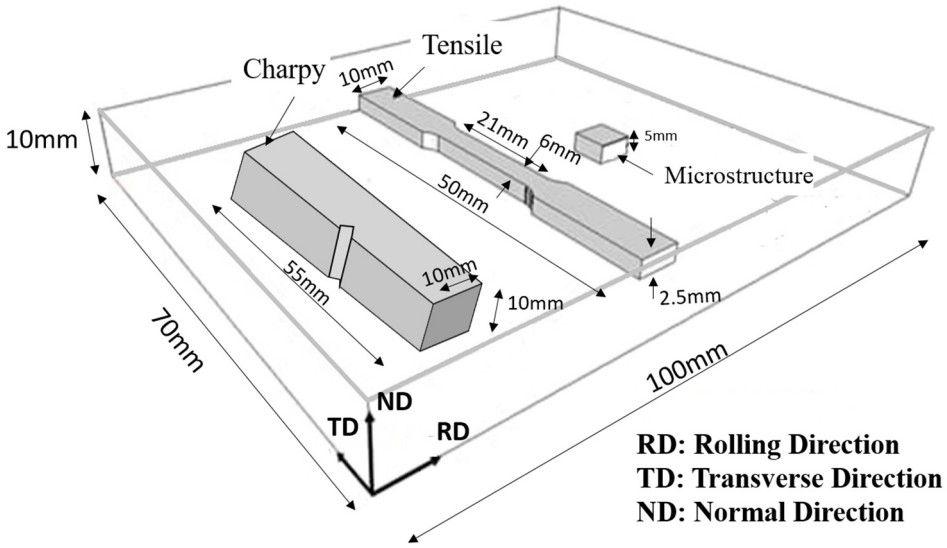


Figure 1. Schematic representation of the samples used for the different microstructural analysis and mechanical testing with respect to rolled and heat-treated plate.

3. Results

3.1. Microstructural Characterization

The microstructural characterization performed on the investigated steels is reported in detail in our previous article [19]. Some of the important microstructural observations are summarized below.

- The investigated specimens display a tempered lath martensitic structure, with finer PAG and packet sizes in B-free steel compared to B-added steels, indicating boron's role in stabilizing the microstructure;
- With an increase in the austenitization temperature (AT), the PAG size increases in all the steels. It was found that 70 ppm B steel shows the minimum variation in the PAG size, packet size and lath width with a change in AT, followed by 100 ppm B steel. However, the 25 ppm B and 90 ppm B steels show a significant increase in the PAG size (>50 μm) and packet size (>30 μm) with an increase in AT. Optical micrographs showing the change in the prior austenite grain size (PAGS) of 100 ppm B steel with the increase in AT are presented in Figure 2a–c;
- The low-angle boundaries (LABs) were sub-grain boundaries (particularly in B-free steel) and lath boundaries (in B-containing steels). The fraction of LABs (2–15° misorientation angle), estimated from the EBSD analysis, was found to be at the maximum in the 1000 °C-austenitized B-free specimen and decreased with the increase in AT. The same trend was also followed by the 100 ppm B steel. In contrast, the 70 ppm B steel displayed the minimum existence of LABs for 1000 °C AT, whilst it reached the maximum value at 1100 °C AT;
- High-angle grain boundaries (HABs) comprised PAG boundaries, a packet and block boundaries. The HABs of B-free steel were consistently high for all the ATs (due to the refined grain structure). It was found that 70–100 ppm B steels revealed a consistently low occurrence of HABs that remained stable with AT. The density of HABs decreased linearly with the increase in AT for the 25 ppm B steel. At 1100 °C, both the 25 ppm B steel and the 90 ppm B steel reached the minimum intensity of HABs;
- Undissolved precipitates were more prevalent in samples austenitized at lower temperatures, mainly due to the decreased likelihood of the pre-existing precipitates dissolving at lower temperatures. After austenitizing at a higher temperature (1100 °C), $M_{23}C_6$-type precipitates completely dissolved, while only partially or undissolved MX

precipitates were retained. During the subsequent tempering, the dissolved solute atoms formed fresh and fine precipitates. SEM ($M_{23}C_6$ precipitates) and TEM ($M_{23}C_6$ and MX precipitates) images, showing precipitates formed after tempering, are exhibited in Figure 2d–i. For a lower AT, the undissolved precipitates tend to coarsen during tempering;

- As the AT increases, there is a reduction in the average precipitate size (>50 nm; mostly $M_{23}C_6$) and an increase in the volume fraction after the tempering treatment;
- Among the B-added steels, 100 ppm B steel possesses the smallest precipitate size, whereas the 70 ppm B steel exhibits larger precipitates and a higher volume fraction, regardless of the AT, compared to other B-added steels;
- The AES study confirms the segregation of B exactly at the precipitates in all the steels nearby PAG boundaries and sub-grain boundaries closer to the PAG boundaries.

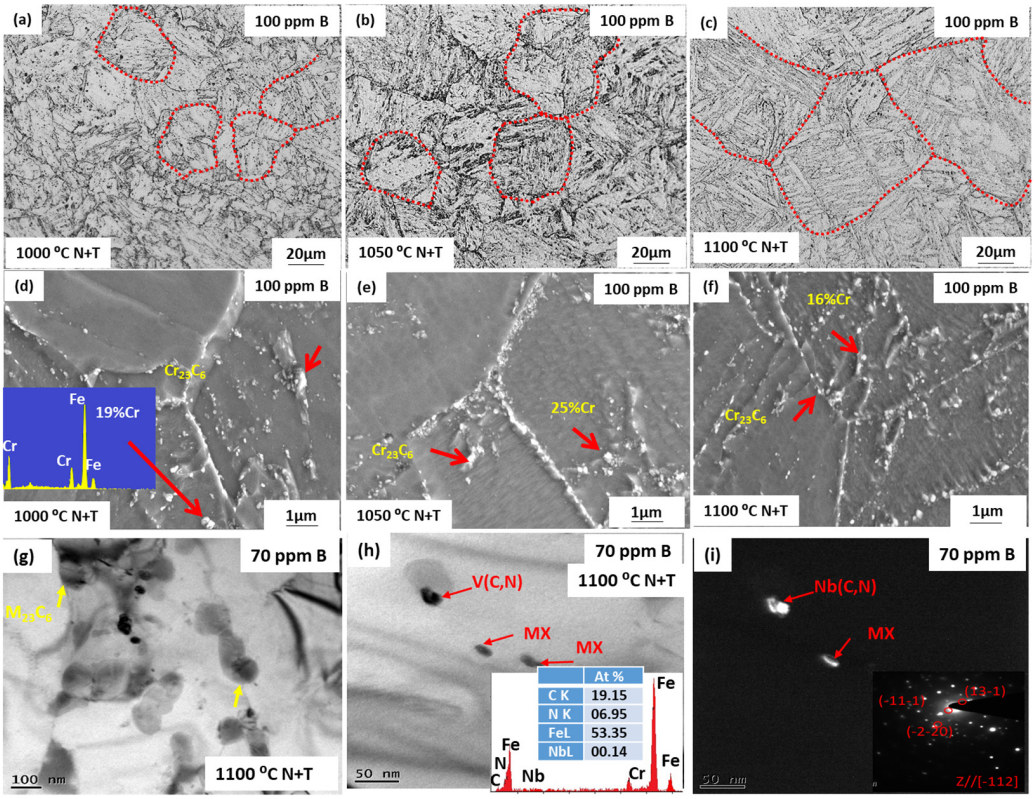


Figure 2. (**a**–**c**) Optical micrographs (PAG boundaries delineated) and corresponding (**d**–**f**) SEM micrographs (marking the $M_{23}C_6$ precipitates nearby PAG boundaries) of 100 ppm B steel with a change in AT. (**g**–**i**) TEM of 70 ppm B steel austenitized at 1100 °C followed by tempering. MX, $M_{23}C_6$ precipitates are marked, and heat treatment conditions are shown as well. SADP and EDS results are also included as insets, wherever necessary.

All of the above findings reported need to be correlated with tensile and impact testing results to understand the influence of alloying elements, precipitates and the microstructure.

Figure 3 presents the AES results for B segregation in 100 ppm B steel under different heat treatment conditions. In the as-normalized condition (N), B segregated preferentially at PAG boundaries and nearby lath boundaries. B segregation was higher in the specimen austenitized at 1100 °C (as shown in Figure 3a,b) compared to the specimen austenitized at a lower temperature of 1000 °C (Figure 3c,d). As a note, B segregation near PAG boundaries usually promotes the formation of B-rich precipitates ($M_{23}(B,C)_6$) during subsequent tempering [34–37]. The enrichment of B in the $(Fe,Cr)_{23}C_6$ precipitates after the tempering treatment is evidenced in Figure 3e–h in 100 ppm B and 70 ppm B steels (also elucidated in [19]). The B enrichment in the $M_{23}(B,C)_6$ precipitates reduces the coarsening rate of those precipitates.

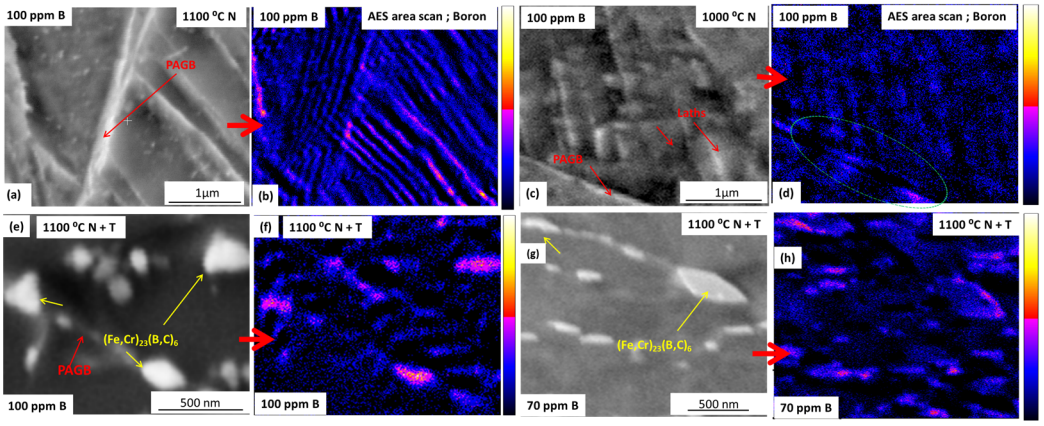


Figure 3. AES results showing B segregation along the PAG boundaries in 100 ppm B steel after the normalization treatment for (**a**,**b**) a 1100 °C austenitization temperature and (**c**,**d**) a 1000 °C austenitization temperature. B enrichment in the $(Fe,Cr)_{23}C_6$ precipitates after the tempering treatment of 1100 °C N samples is shown in (**e**,**f**) for 100 ppm B steel and in (**g**,**h**) for 70 ppm B steel.

3.2. Tensile Properties of the Investigated Steels

The engineering stress vs. strain curves of the investigated steels for 1000 °C and 1100 °C normalized and tempered conditions are shown in Figure 4, and the tensile properties are listed in Table 2.

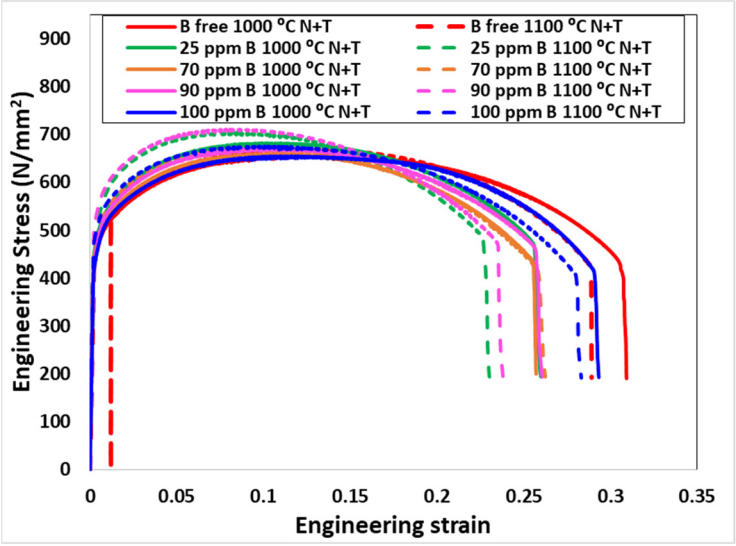


Figure 4. Engineering stress–strain curves of all the investigated steels after normalization followed by tempering (1000/1100 °C N+T). Austenitization condition and steel codes are shown in legends.

Table 2. Tensile properties of the investigated steels after normalization followed by tempering (1000/1100 °C N+T).

Tensile Properties *	B-free		25 ppm B		70 ppm B		90 ppm B		100 ppm B	
	1000 °C N+T	1100 °C N+T	1000 °C N+T	1100 °C N+T	1000 °C N+T	1100 °C N+T	1000 °C N+T	1100 °C N+T	1000 °C N+T	1100 °C N+T
YS	458.1 ± 5	467.9 ± 6	490.6 ± 6	511.2 ± 7	478.1 ± 6	490.4 ± 4	474.3 ± 11	542.5 ± 9	457.2 ± 12	512.7 ± 10
UTS	656.1 ± 6	669.4 ± 4	682.6 ± 5	705.0 ± 5	660.2 ± 4	670.5 ± 5	671.4 ± 8	710.9 ± 11	655.5 ± 9	676.2 ± 6
%EL	30.5 ± 1.1	28.9 ± 0.9	25.6 ± 0.9	22.7 ± 0.7	25.9 ± 1.2	25.9 ± 0.8	25.6 ± 0.5	23.5 ± 0.8	29.1 ± 1.2	28.0 ± 1.4
n	0.137	0.1479	0.1393	0.1332	0.137	0.1327	0.1423	0.1213	0.1423	0.1231

* Tests were repeated, and the deviations in measurements were within 5%.

The important observations are as follows.

- All the steels austenitized at 1100 °C possess superior tensile strength as compared to those austenitized at 1000 °C;
- B-containing steels possess higher *YS* and *UTS* compared to B-free steel irrespective of the austenitizing conditions;
- The B-free steel that was austenitized at 1000 °C exhibited the lowest *YS* (458 MPa) and *UTS* (656 MPa), whereas the highest *YS* (543 MPa) and *UTS* (711 MPa) were observed in the 90 ppm B steel after austenitizing at 1100 °C. The strength of the steel is as follows: 90 ppm B > 25 ppm B > 100 ppm B > 70 ppm B > B-free;
- Compared to other B-containing steels, the 100 ppm B steel displays good tensile strength and significant ductility. However, at 1100 °C, the 25 ppm B and 90 ppm B steels exhibit the highest tensile strength, but they have the least ductility among all the steel types and heat treatment conditions, with only 23% and 24% total elongation, respectively. Among the steels heat-treated at 1000 °C, both these steels exhibit the lowest ductility (26% each). B-free has the highest percentage elongation, measuring 31% and 29% at 1000 °C and 1100 °C, respectively, followed by the 100 ppm B steel, with 29% total elongation at 1000 °C and 28% at 1100 °C.

3.3. Charpy Impact Properties

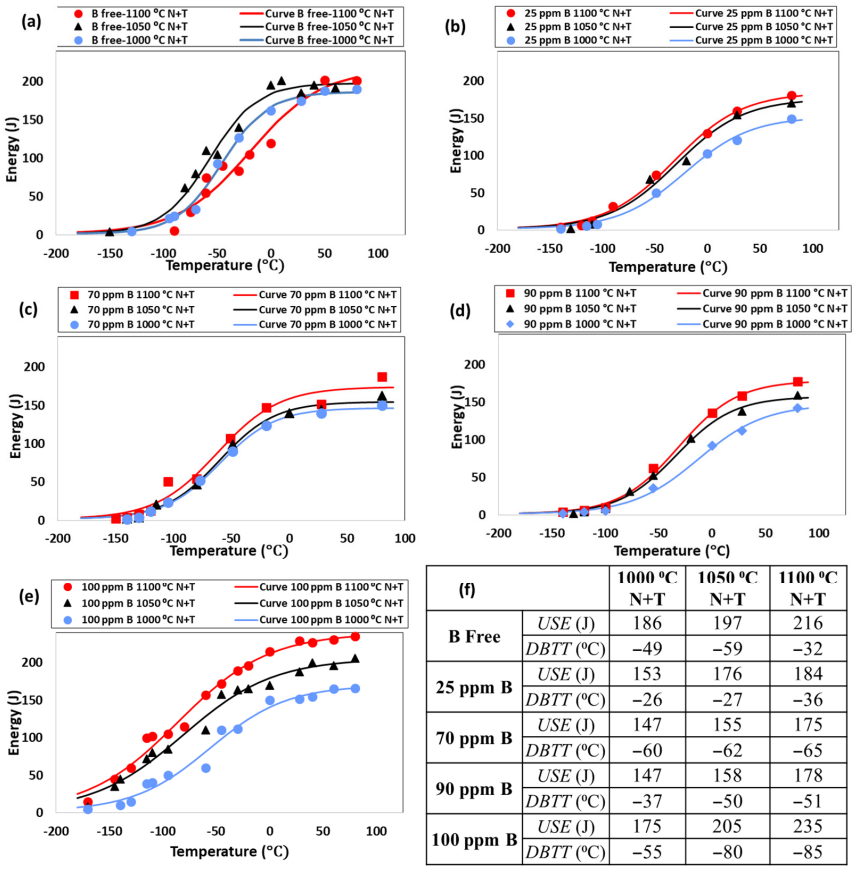
The Charpy impact transition curves of the B-free and B-added steels for different N+T conditions are shown in Figure 5. All the transition curves were fitted with the 'tanh' function in the equation below using the data measured via the Charpy impact testing.

$$C_v = A + B \times \tanh \times ((T - T_0)/C) \quad (2)$$

where A, B and C are constants, T = testing temperature and T_0 = ductile–brittle transition temperature (*DBTT*) estimated from the mean of the corresponding impact energy observed in the upper shelf region (*USE*) and lower shelf region (*LSE*) [38]. The major findings observed from the curves are listed below:

- The impact properties of 100 ppm B steel appear to be superior although more sensitive to heat treatment conditions compared to those of the other steels. In the case of 100 ppm B steel, the *USE* and *DBTT* vary over a wider range with the increase in AT (175 J to 235 J *USE* with −55 °C to −85 °C *DBTT*);
- Among the austenitization temperatures, all the B-added steels show the best impact properties at 1100 °C AT, in which 100 ppm B steel possesses the lowest *DBTT* (−85 °C), followed by 70 ppm B (−65 °C), 90 ppm B (−51 °C) and 25 ppm B (−36 °C);
- At a lower AT (1000 °C N+T), the 70 ppm B steel possesses the lowest *DBTT* (−60 °C). Moreover, the least change in *DBTT* (−60 °C to −65 °C) and *USE* (147 J to 175 J) with increasing AT was observed in 70 ppm B steel among the investigated steels;
- The *USE* values of 25 ppm B and 90 ppm B steels vary from 153 J to 184 J and from 147 J to 178 J, respectively, with increasing AT;
- For B-free steel, the best impact properties were obtained at 1050 °C AT, with lower *USE* (197 J) and considerably lower *DBTT* (−59 °C) compared to those of the 1100 °C AT sample (216 J *USE*, −32 °C *DBTT*).

Figure 6 displays the fracture surfaces of the Charpy impact-tested 100 ppm B steels, which depict a transition from the purely ductile mode of fracture at higher temperatures to the mixed mode at intermediate temperatures and the purely brittle mode of fracture at very low temperatures. Different arrows are shown in each regime. The red arrows indicate the presence of cleavage facets, which indicates the brittle mode of fracture, especially for the micrographs from the lower shelf region containing numerous facets along with de-cohesion along the PAG boundaries. The presence of cleavage facets and dimples (green arrows) represents the transition zone or the brittle-to-ductile transition of the fracture surface, and it becomes completely ductile (only green arrows) once it reaches the upper shelf region of the transition curve.



(f)		1000 °C N+T	1050 °C N+T	1100 °C N+T
B Free	*USE* (J)	186	197	216
	DBTT (°C)	−49	−59	−32
25 ppm B	*USE* (J)	153	176	184
	DBTT (°C)	−26	−27	−36
70 ppm B	*USE* (J)	147	155	175
	DBTT (°C)	−60	−62	−65
90 ppm B	*USE* (J)	147	158	178
	DBTT (°C)	−37	−50	−51
100 ppm B	*USE* (J)	175	205	235
	DBTT (°C)	−55	−80	−85

Figure 5. Ductile–brittle transition curves (Charpy impact energy vs. temperature) of the investigated steels normalized at 1000/1050/1100 °C for 1 h followed by tempering at 760 °C for 1 h of (**a**) B-free steel, (**b**) 25 ppm B steel, (**c**) 70 ppm B steel, (**d**) 90 ppm B steel and (**e**) 100 ppm B steel. (**f**) Table showing the upper shelf energy and *DBTT* of all the investigated steels.

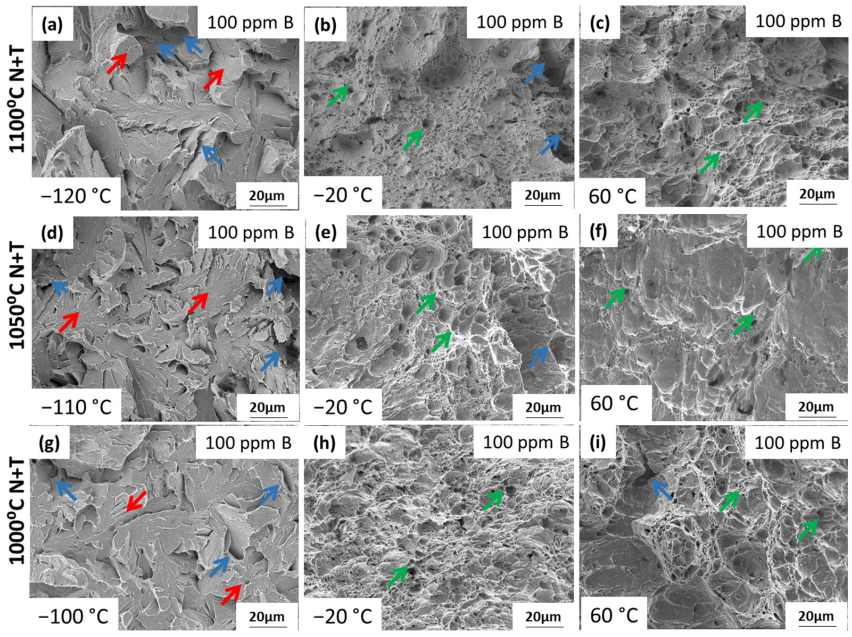


Figure 6. (**a**–**i**) Fractographs of Charpy impact-tested specimens from different zones of the ductile-to-brittle transition curve generated for 100 ppm B steels. Blue, Red and Green arrows represent decohesion along PAG boundaries, cleavage facets and ductile dimples, respectively. The heat-treatment condition, Charpy impact testing temperature and steel codes are marked in each micrograph.

4. Discussion

Superior tensile properties at higher austenitization temperatures can be attributed to the proper dissolution of pre-existing precipitates and the formation of finer precipitates during tempering. Figure 7 depicts the detailed characterization of both the $M_{23}C_6$ and MX undissolved precipitates observed in the TEM study, confirmed using energy dispersive spectroscopy (EDS) and the selected area diffraction pattern (SADP) on the steels after normalizing (i.e., before tempering). As the AT decreases, there is an increase in the number of undissolved precipitates that tend to coarsen during tempering, leading to a deterioration in strength. Additionally, highly stable MX nitrides/carbides containing mainly V and Nb also significantly contributed to precipitation strengthening. MX nitrides possess a higher stability than MX carbides, and 70 ppm B steel contains the highest fraction of N among the B-containing steels.

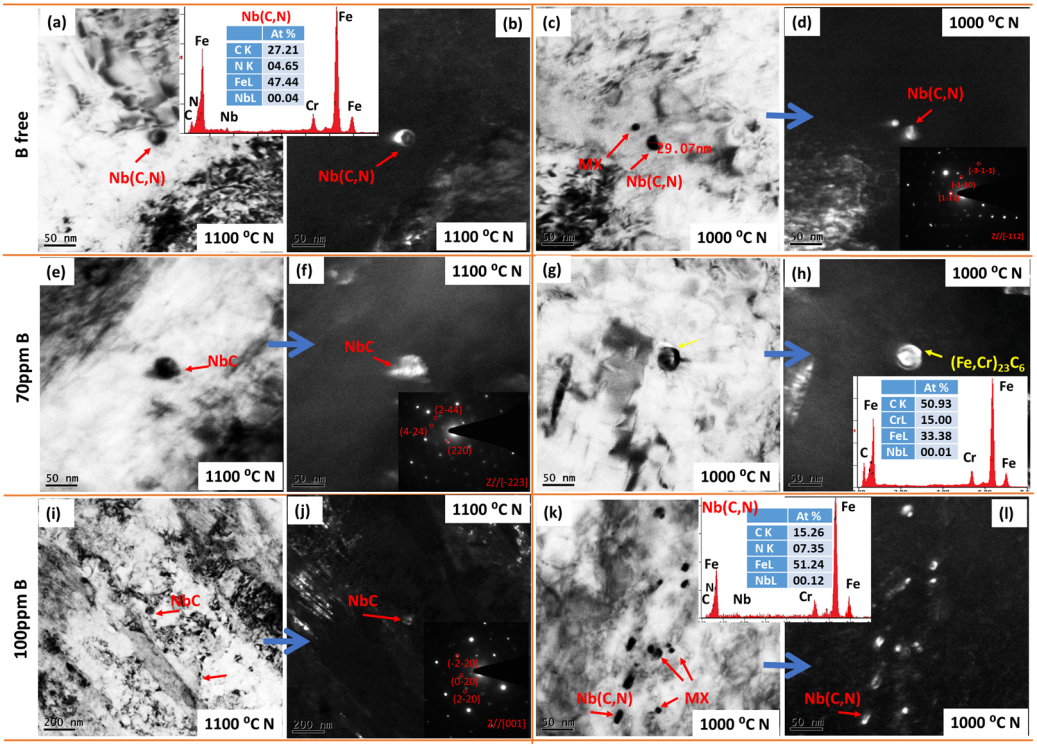


Figure 7. TEM bright field and dark field images of (**a**–**d**) B-free, (**e**–**h**) 70 ppm B and (**i**–**l**) 100 ppm B steels after austenitization at 1000/1100 °C (N). Different undissolved precipitates are marked based on their corresponding EDS data (shown as table insets) and SAD patterns.

In 100 ppm B steel, even though the C content is less (0.10 wt.%), the finest $(Fe,Cr)_{23}(B,C)_6$ precipitates (with the highest fraction) along with a relatively low fraction of coarser $Cr_{23}C_6$ contributed to the good strength for both austenitization conditions, particularly at 1100 °C AT. Despite the highest C content (0.15 wt.%) and sufficient N content (108 ppm) present in the 70 ppm B steel, a moderate tensile strength and ductility were observed, possibly due to the largest average $M_{23}C_6$ precipitate size among the B-containing steels. The higher N content in 25 ppm B and 90 ppm B steels (both 90 ppm N) compared to that in 100 ppm B steel (20 ppm N) can potentially form a higher fraction of MX nitrides along with B-containing carbides, resulting in a superior tensile strength. At the same time, a comparatively higher C content (0.11 and 0.13 wt.%) might possibly reduce the ductility. Additionally, the 70 ppm B steel showed the least change in the *YS*, *UTS* and percentage elongation with AT, which can be attributed to the consistent microstructural features. In B-free steel, the average $M_{23}C_6$ size was measured to be the highest irrespective of the austenitization condition, which possibly reduced its tensile strength.

The presence of elements such as C and Cr, which dissolved during austenitization, promotes solid solution strengthening in steels and can lower the impact toughness. It was found that 70 ppm B steel contains a higher fraction of both C and Cr compared to other steels, and this may have reduced the impact energy absorbed in the upper shelf region of the transition curve. The 100 ppm B steel has the least amount of C and Cr; hence, the effect of solid solution strengthening is reduced. Consequently, it exhibits the highest upper shelf energy and lowest *DBTT* among all the steels investigated. The addition of Ni is beneficial for impact properties [3], and 70 ppm B steel has the least amount of Ni, which may have not contributed enough for better impact properties. Similarly, B-free steel also possesses good impact properties owing to its low C and Cr content as well as a higher Ni content. The 25 ppm B and 90 ppm B steels contain a lower amount of Cr and a higher amount of Ni than the 70 ppm B steel, which resulted in a slight improvement in the impact energy absorbed.

Auger electron spectroscopy (in Figure 3) confirmed the segregation of B and the formation of B-enriched precipitates, which are more stable and fine than the B-free $M_{23}C_6$ precipitates [19]. The formation of $(Fe,Cr)_{23}(B,C)_6$ reduces the $Cr_{23}C_6$ fraction, and these precipitates along with a small fraction of fine MX precipitates restrict the prior austenite grain refinement during the austenitization of B-added steels. The stabilization of fine precipitates along the martensite lath (and block) boundaries facilitates the growth of austenite as fine films leading to the reconstruction of PAG [34,35,39]. During the progress of austenite reversion, the austenite films grow rapidly (possibly following a shear transformation mechanism) and consume the martensite block, within which the laths are situated. Thus, austenite films grow 'block-by-block', finally coalescing with each other to reconstruct the entire PAG. The retention of fine and stable precipitates along the lath boundaries further ensures the transformation of austenite into a lath martensite structure upon cooling instead of a sub-grain structure. Thus, stable $(Fe,Cr)_{23}(B,C)_6$ precipitates can lead to a coarser PAG and packet size in B-containing steels, which can reduce the fraction of HABs. Now, the HABs are known to retard and divert the cleavage crack propagation, particularly at low test temperatures, and a finer PAG structure can be beneficial in this respect [9]. However, in B-free steel, although the PAG size is fine, mostly, a sub-grain structure formed (with a high density of low-angle sub-boundaries), as the lath martensite structure could not be retained due to the lower precipitate stability. The LABs are ineffective in retarding the cleavage crack propagation. The B-free steel also contained coarser precipitates, which lowered the precipitation strengthening contribution and, consequently, the overall strength. A lower strength is expected to promote plastic deformation and improve the impact toughness, particularly at the upper shelf region. As a result, B-free steel showed relatively higher *USE* and an intermediate *DBTT*.

The best impact properties (high *USE* and low *DBTT*) of 100 ppm B steel can be attributed to (i) the fine precipitate size (due to the B stabilization effect) and (ii) the low fraction of MX precipitates (due to the low N content). The fractions of $M_{23}C_6$ and MX precipitates are predicted by Thermo-Calc® software for the investigated steel compositions and are reported in our previous study [19]). Fine precipitates nucleate small voids, and the scope for the sufficient growth of those voids contributes to the impact toughness. Fine precipitates are also less prone to initiating cleavage crack than coarse precipitates. The lower precipitation strengthening can also be beneficial for toughness. The best impact properties of 100 ppm B steel (with just 20 ppm N) indicate the dominant role of the precipitate size and fraction on the impact toughness compared to the microstructural refinement in the B-added P91 steels. In spite of the high precipitate and microstructural stability, 70 ppm B steel contained relatively coarser $M_{23}C_6$ precipitates and a higher fraction of MX precipitates than 100 ppm B steel. Therefore, the impact properties of 70 ppm B steel were not as good as those of 100 ppm B steel. The combination of the precipitate size and fraction (and the extent of microstructural refinement) also resulted in inferior impact properties of 25 ppm and 90 ppm B steels as compared to those of 100 ppm

B steel. Thus, the impact properties obtained in the present study contradict the findings of Mishnev et al. [30].

Besides the level of *DBTT*, its variation with AT is different between B-free steel (lowest *DBTT* at an intermediate AT of 1050 °C) and the B-containing steels (decrease in *DBTT* with the increase in AT). In B-free P91 steel, Chatterjee et al. [9] also obtained the lowest *DBTT* at the intermediate AT (1025 °C). Such a finding can be explained by the optimum precipitate size and grain size ('effective grain size' in this case) at an intermediate AT, since the precipitates become coarse at a low AT, whilst the grains become coarse at a high AT. In B-containing steels, precipitates appear to govern the impact properties, and, hence, *DBTT* decreases with the increase in AT. The presence of undissolved precipitates at a lower AT and the subsequent coarsening of those precipitates during tempering were detrimental to the impact toughness. At higher testing temperatures, where the ductile fracture dominates, the coarse precipitates nucleate large voids which coalesce into cracks without sufficient growth, thereby lowering the impact toughness. On the other side, at lower test temperatures, coarse particles can act as the initiation sites for cleavage cracks, again affecting the toughness.

5. Conclusions

After performing different microstructural characterization and mechanical testing, the main points are summarized below.

- The B-free steel possesses the best ductility (%*EL*) among all the investigated steels (including the austenitization temperature, AT and variation) but poor *YS* and *UTS*. The poor strength of B-free steel is mainly attributed to the presence of large, undissolved $M_{23}C_6$ and MX precipitates. The lower C and Cr contents as well as the higher Ni content in B-free steel greatly contributed to its high ductility as well as good impact properties (mainly the *USE*). Moreover, the high fraction of HAB (due to refined PAGs) in the B-free steel greatly improves the low temperature impact toughness, which thereby results in a lower *DBTT*;
- In the B-containing steels, both the strength as well as the impact properties are mainly controlled by the precipitate characteristics rather than the PAG size. Increasing the AT dissolves the coarse $M_{23}C_6$ precipitates, while increasing the B content helps in stabilizing the formation of fine B-rich $(Fe,Cr)_{23}(B,C)_6$ precipitates during the subsequent tempering. Increasing the N content results in larger and more abundant MX precipitates that are detrimental for toughness. As a whole, the presence of a high fraction of fine $(Fe,Cr)_{23}(B,C)_6$ precipitates and low fractions of coarse $M_{23}C_6$ and MX precipitates leads to an enhanced strength–impact toughness combination, which can be achieved by increasing the AT and B content and decreasing the N content of the B-added P91 steels;
- The 100 ppm B steel (containing the maximum B and minimum N), normalized at the maximum AT of 1100 °C, shows the best combination of tensile properties (*YS*: 513 MPa, *UTS*: 676 MPa and %*EL*: 28 %) and Charpy impact properties (*USE*: 235 J and *DBTT*: −85 °C), owing to the abundance of fine B-rich $(Fe,Cr)_{23}(B,C)_6$ precipitates and the deficiency of coarse $M_{23}C_6$ and MX precipitates.

Author Contributions: Conceptualization, D.C.; methodology, R.R.; validation, D.C.; formal analysis, R.R. and D.C.; investigation, R.R.; resources, R.M., C.R.D. and D.C.; writing—original draft preparation, R.R.; writing—review and editing, R.K.B., R.M., A.K., C.R.D. and D.C.; supervision, R.M., C.R.D., S.K.A. and D.C.; funding acquisition, S.K.A. and A.K. All authors have read and agreed to the published version of the manuscript.

Funding: This research was funded by the Board of Research in Nuclear Sciences (BRNS) (Sanction No. 36(2)/14/26/2016-BRNS/36026, Dated: 8 July 2016).

Data Availability Statement: The raw/processed data required to reproduce these findings cannot be shared at this time, as the data also form part of an ongoing study.

Acknowledgments: Most of the experiments were performed using the facilities from IIT Kharagpur, and the entire project was funded by the Board of Research in Nuclear sciences (BRNS). Throughout the entire work, the Indira Gandhi Center for Atomic Research, IGCAR Kalpakkam (Project collaborator) supported with valuable guidance. The authors acknowledge all the support received for the completion of this work.

Conflicts of Interest: The authors declare no conflict of interest.

References

1. Saini, N.; Pandey, C.; Mohan, M.; Narang, H.K.; Mulik, R.S.; Kumar, P. A Comparative Study of Ductile-Brittle Transition Behavior and Fractography of P91 and P92 Steel. *Eng. Fail. Anal.* **2017**, *81*, 245–253. [CrossRef]
2. Kim, S.H.; Yoon, J.; Ryu, W.S.; Lee, C.B.; Hong, J.H. Fracture Toughness of Irradiated Modified 9Cr—1Mo Steel. *J. Nucl. Mater.* **2009**, *386–388*, 387–389. [CrossRef]
3. Bhaduri, A.K. Development and Deployment of Welding Technologies for the Indian Sodium-Cooled Fast Reactor and Advanced Ultra-Supercritical Thermal Power Programmes. *Trans. Indian Inst. Met.* **2021**, *74*, 1035–1053. [CrossRef]
4. Chakraborty, G.; Rejeesh, R.; Ramana, O.V.; Albert, S.K. Evaluation of Hydrogen-Assisted Cracking Susceptibility in Modified 9cr-1mo Steel Welds. *Weld. World* **2020**, *64*, 115–122. [CrossRef]
5. Dak, G.; Pandey, C. A Critical Review on Dissimilar Welds Joint between Martensitic and Austenitic Steel for Power Plant Application. *J. Manuf. Process.* **2020**, *58*, 377–406. [CrossRef]
6. Guo, X.; Gong, J.; Jiang, Y.; Rong, D. The Influence of Long-Term Aging on Microstructures and Static Mechanical Properties of P92 Steel at Room Temperature. *Mater. Sci. Eng. A* **2013**, *564*, 199–205. [CrossRef]
7. Zhang, L.; Yu, L.; Liu, Y.; Liu, C.; Li, H.; Wu, J. Influence of Zr Addition on the Microstructures and Mechanical Properties of 14Cr ODS Steels. *Mater. Sci. Eng. A* **2017**, *695*, 66–73. [CrossRef]
8. Dong, H.; Yu, L.; Liu, Y.; Liu, C.; Li, H.; Wu, J. Effect of Hafnium Addition on the Microstructure and Tensile Properties of Aluminum Added High-Cr ODS Steels. *J. Alloys Compd.* **2017**, *702*, 538–545. [CrossRef]
9. Chatterjee, A.; Chakrabarti, D.; Moitra, A.; Mitra, R.; Bhaduri, A.K. Effect of Normalization Temperatures on Ductile-Brittle Transition Temperature of a Modified 9Cr-1Mo Steel. *Mater. Sci. Eng. A* **2014**, *618*, 219–231. [CrossRef]
10. Chatterjee, A.; Chakrabarti, D.; Moitra, A.; Mitra, R.; Bhaduri, A.K. Effect of Deformation Temperature on the Ductile-Brittle Transition Behavior of a Modified 9Cr-1Mo Steel. *Mater. Sci. Eng. A* **2015**, *630*, 58–70. [CrossRef]
11. Pandey, C.; Giri, A.; Mahapatra, M.M. Materials Science & Engineering A Evolution of Phases in P91 Steel in Various Heat Treatment Conditions and Their Effect on Microstructure Stability and Mechanical Properties. *Mater. Sci. Eng. A* **2016**, *664*, 58–74. [CrossRef]
12. Takahashi, J.; Ishikawa, K.; Kawakami, K.; Fujioka, M.; Kubota, N. Atomic-Scale Study on Segregation Behavior at Austenite Grain Boundaries in Boron- and Molybdenum-Added Steels. *Acta Mater.* **2017**, *133*, 41–54. [CrossRef]
13. Ueno, M.; Kametarou, I. New Empirical Formula for Estimation of Hardenability from Chemical Compositions. *ISIJ Int.* **1987**, *74*, 133–140.
14. Das, C.R.; Albert, S.K.; Swaminathan, J.; Bhaduri, A.K.; Raj, B.; Murty, B.S. Improvement in Creep Resistance of Modified 9Cr-1Mo Steel Weldment by Boron Addition. *Weld. World* **2012**, *56*, 10–17. [CrossRef]
15. Deva, A.; Jha, B.K.; Mishra, N.S. Influence of Boron on Strain Hardening Behaviour and Ductility of Low Carbon Hot Rolled Steel. *Mater. Sci. Eng. A* **2011**, *528*, 7375–7380. [CrossRef]
16. Sahara, R.; Matsunaga, T.; Hongo, H. Theoretical Investigation of Stabilizing Mechanism by Boron in Body-Centered Cubic Iron Through (Fe, Cr) 23 (C, B) 6 Precipitates. *Metall. Mater. Trans. A* **2016**, *47*, 2487–2497. [CrossRef]
17. Kobayashi, S.; Toshimori, K.; Nakai, K.; Ohmori, Y.; Asahi, H.; Muraki, T. Effects of Boron Addition on Tempering Processes in an Fe-9Cr-0.1C Alloy Martensite. *ISIJ Int.* **2002**, *42*, 72–76. [CrossRef]
18. Blazek, K.-E.; Lanzi, O.; Yin, H. Boron Effects on the Solidification of Steel during Continuous Casting. *Rev. Métallurgie* **2008**, *105*, 609–625. [CrossRef]
19. Rejeesh, R.; Bhattacharya, A.; Haldar, C.; Mitra, R.; Chakrabarti, D.; Das, C.R.; Albert, S.K.; Bhaduri, A.K. Relative Effect of B and N Concentrations on the Microstructural Stability and Mechanical Properties of Modified 9Cr-1Mo Steel. *J. Alloys Compd.* **2021**, *867*, 158971. [CrossRef]
20. Hofer, P.; Miller, M.K.; Babu, S.S.; David, S.A.; Cerjak, H. Atom Probe Field Ion Microscopy Investigation of Boron Containing Martensitic 9 Pct Chromium Steel. *Metall. Mater. Trans. A Phys. Metall. Mater. Sci.* **2000**, *31*, 975–984. [CrossRef]
21. Seol, J.B.; Lim, N.S.; Lee, B.H.; Renaud, L.; Park, C.G. Atom Probe Tomography and Nano Secondary Ion Mass Spectroscopy Investigation of the Segregation of Boron at Austenite Grain Boundaries in 0.5 Wt.% Carbon Steels. *Met. Mater. Int.* **2011**, *17*, 413–416. [CrossRef]
22. Li, Y.J.; Ponge, D.; Choi, P.; Raabe, D. Segregation of Boron at Prior Austenite Grain Boundaries in a Quenched Martensitic Steel Studied by Atom Probe Tomography. *Scr. Mater.* **2015**, *96*, 13–16. [CrossRef]
23. Da Rosa, G.; Maugis, P.; Portavoce, A.; Drillet, J.; Valle, N.; Lentzen, E.; Hoummada, K. Grain-Boundary Segregation of Boron in High-Strength Steel Studied by Nano-SIMS and Atom Probe Tomography. *Acta Mater.* **2020**, *182*, 226–234. [CrossRef]

24. Abe, F. Precipitate Design for Creep Strengthening of 9% Cr Tempered Martensitic Steel for Ultra-Supercritical Power Plants. *Sci. Technol. Adv. Mater.* **2008**, *9*, 013002. [CrossRef] [PubMed]
25. Rietema, C.J.; Hassan, M.M.; Anderoglu, O.; Eftink, B.; Saleh, T.A.; Maloy, S.A.; Clarke, A.J.; Clarke, K.D. Ultrafine Intralath Precipitation of V(C,N) in 12Cr-1MoWV (Wt.%) Ferritic/Martensitic Steel. *Scr. Mater.* **2021**, *197*, 113787. [CrossRef]
26. Abe, F.; Horiuchi, T.; Taneike, M.; Sawada, K. Stabilization of Martensitic Microstructure in Advanced 9Cr Steel during Creep at High Temperature. *Mater. Sci. Eng. A* **2004**, *378*, 299–303. [CrossRef]
27. Sakuraya, K.; Okada, H.; Abe, F. BN Type Inclusions Formed in High Cr Ferritic Heat Resistant Steel. *Energy Mater.* **2006**, *1*, 158–166. [CrossRef]
28. Lu, Y. Effect of Boron on Microstructure and Mechanical Properties of PM Sintered and Nitrided Steels. Ph.D. Thesis, Department of Mining, Metals and Materials Engineering, McGill University Montreal, Montreal, QC, Canada, 2003. Volume 44.
29. Dudova, N.; Mishnev, R.; Kaibyshev, R. Effect of Tempering on Microstructure and Mechanical Properties of Boron Containing 10%Cr Steel. *ISIJ Int.* **2011**, *51*, 1912–1918. [CrossRef]
30. Mishnev, R.; Dudova, N.; Dudko, V.; Kaibyshev, R. Impact Toughness of a 10% Cr Steel with High Boron and Low Nitrogen Contents. *Mater. Sci. Eng. A* **2018**, *730*, 1–9. [CrossRef]
31. *ASTM A213*; Tubing Standard Specification (ASME SA213) Standard Specification for Seamless Ferritic and Austenitic Alloy-Steel Boiler, Superheater, and Heat-Exchanger Tubes, Annu. B. ASTM Stand. ASTM International: West Conshohocken, PA, USA, 2006; pp. 1–12.
32. *ASTM E8/E8M*; Standard Test Methods for Tension Testing of Metallic Materials 1. ASTM International: West Conshohocken, PA, USA, 2010; pp. 1–27.
33. *ASTM E 23-12c*; Standard Test Methods for Notched Bar Impact Testing of Metallic Materials. ASTM International: West Conshohocken, PA, USA, 2012; pp. 1–25.
34. Fedorova, I.; Liu, F.; Grumsen, F.B.; Cao, Y.; Mishin, O.V.; Hald, J. Fine (Cr,Fe)2B Borides on Grain Boundaries in a 10Cr–0.01B Martensitic Steel. *Scr. Mater.* **2018**, *156*, 124–128. [CrossRef]
35. Abe, F.; Taneike, M.; Sawada, K. Alloy Design of Creep Resistant 9Cr Steel Using a Dispersion of Nano-Sized Carbonitrides. *Int. J. Press. Vessel. Pip.* **2007**, *84*, 3–12. [CrossRef]
36. Das, C.R.; Albert, S.K.; Bhaduri, A.K.; Murty, B.S. Effect of Boron Addition and Initial Heat-Treatment Temperature on Microstructure and Mechanical Properties of Modified 9Cr-1Mo Steels under Different Heat-Treatment Conditions. *Metall. Mater. Trans. A Phys. Metall. Mater. Sci.* **2013**, *44*, 2171–2186. [CrossRef]
37. Khajuria, A.; Akhtar, M.; Bedi, R.; Kumar, R.; Ghosh, M.; Das, C.R.; Albert, S.K. Influence of Boron on Microstructure and Mechanical Properties of Gleeble Simulated Heat-Affected Zone in P91 Steel. *Int. J. Press. Vessel. Pip.* **2020**, *188*, 104246. [CrossRef]
38. Dieter, G.E. *Mechanical Metallurgy*; McGraw Hill: New York, NY, USA, 2011.
39. Golpayegani, A.; Liu, F.; Svensson, H.; Andersson, M.; Andrén, H.O. Microstructure of a Creep-Resistant 10 Pct Chromium Steel Containing 250 Ppm Boron. *Metall. Mater. Trans. A Phys. Metall. Mater. Sci.* **2011**, *42*, 940–951. [CrossRef]

Disclaimer/Publisher's Note: The statements, opinions and data contained in all publications are solely those of the individual author(s) and contributor(s) and not of MDPI and/or the editor(s). MDPI and/or the editor(s) disclaim responsibility for any injury to people or property resulting from any ideas, methods, instructions or products referred to in the content.